Analytical and Numerical Solutions of a Generalized Hyperbolic Non-Newtonian Fluid Flow

Mehmet Pakdemirli[a], Pınar Sarı[b], and Bekir Solmaz[b]

[a] Department of Mechanical Engineering, Celal Bayar University, 45140 Muradiye, Manisa, Turkey
[b] Department of Civil Engineering, Celal Bayar University, 45140 Muradiye, Manisa, Turkey

Reprint requests to Fax: +90.236.2412143; E-mail: mpak@bayar.edu.tr; pinar.sari@bayar.edu.tr; bekir.solmaz@bayar.edu.tr

Z. Naturforsch. **65a,** 151 – 160 (2010); received February 10, 2009 / revised June 16, 2009

The generalized hyperbolic non-Newtonian fluid model first proposed by Al-Zahrani [J. Petroleum Sci. Eng. **17**, 211 (1997)] is considered. This model was successfully applied to some drilling fluids with a better performance in relating shear stress and velocity gradient compared to power-law and the Hershel-Bulkley model. Special flow geometries namely pipe flow, parallel plate flow, and flow between two rotating cylinders are treated. For the first two cases, analytical solutions of velocity profiles and discharges in the form of integrals are presented. These quantities are calculated by numerically evaluating the integrals. For the flow between two rotating cylinders, the differential equation is solved by the Runge-Kutta method combined with shooting. For all problems, the power-law approximation of the model is compared with the generalized hyperbolic model, too.

Key words: Generalized Hyperbolic Non-Newtonian Fluid; Pipe Flow; Parallel Plate Flow; Flow Between Rotating Cylinders.

1. Introduction

Fluids in petroleum industry usually exhibit non-Newtonian behaviour. Crude oil and drilling fluids are some examples. In non-Newtonian fluids, the shear stress is not linearly related to the velocity gradient. Various models were proposed to express the relationship between the shear stress and the velocity gradient. In the pseudoplastic group power-law, Hershel-Buckley, Ellis, and Eyring models are some examples [2 – 4]. These models cannot account for the normal stresses observed in some of the non-Newtonian fluids. To account for the normal stresses, models such as Oldroy, Maxwell, second-grade and third-grade fluids, the latter two being special forms of the broad class named as Rivlin-Ericksen fluids, were also proposed [5 – 18]. Recently, Al-Zahrani [1] proposed a new pseudoplastic non-Newtonian model in a general hyperbolic form. Experiments with the new model revealed that the model better performs than the power-law and Hershel-Bulkley model in predicting shear stress and velocity gradient relationship of some drilling fluids [1]. Parameter values of the constitutive relation are experimentally detected for some drilling fluids also [1]. In a further study, Al-Zahrani and Al-Fariss [19] modified the model to determine the temperature dependent viscosity of waxy oils and obtained a promising match between the model and the experimental data.

In this work, using the generalized hyperbolic model, three different fluid flow problems are solved: i) pipe flow, ii) flow between parallel plates, and iii) flow between rotating concentric cylinders. For the first two cases, the velocities and discharges are given analytically in the integral form and the integrals are evaluated numerically for various pressure gradients and power index values. For the last case, the outcoming ordinary differential equation is numerically solved using a Runge-Kutta algorithm combined with shooting technique. Solutions are presented for various inside to outside cylinder radii and for various rotation speeds. All solutions corresponding to the three problems are also contrasted with the power-law approximation of the model.

2. Constitutive Relation

The general constitutive relation proposed by Al-Zahrani [1] is

$$\tau^* = \frac{B}{\delta^{1/n}} \left[\left(\frac{\dot{\gamma}^* + \delta A}{A} \right)^n - 1 \right]^{1/n} . \qquad (1)$$

In this general form, the stress constitutive equation is a generalization of Newtonian, power-law, and Hershel-Buckley fluids. δ is a dimensionless parameter. If $\delta = 1$ is selected, then the initial yield stress vanishes and the model does not represent Hershel-Buckley fluids for vanishing velocity gradients. Following [1], $\delta = 1$ is selected in the subsequent analysis and for this choice

$$\tau^* = B\left[\left(\frac{\dot{\gamma}^* + A}{A}\right)^n - 1\right]^{1/n}, \tag{2}$$

where τ^* is the shear stress, $\dot{\gamma}^*$ is the velocity gradient, and A, B, and n are constants to be determined for a specific fluid. For $n = 1$, the model represents the Newtonian fluids

$$\tau^* = \frac{B}{A}\dot{\gamma}^* \tag{3}$$

and the ratio B/A is the usual viscosity in this case. For power-law fluids the constitutive relation is

$$\tau^* = k\dot{\gamma}^{*m}. \tag{4}$$

Direct correlation of A, B, and n with k and m does not exist for specific fluids and is not given in [1]. However, it can be shown that for small velocity gradient ratios $\dot{\gamma}^*/A \ll 1$, (2) reduces to (4). The numerical values of A and $\dot{\gamma}^*$ presented in the figures in [1] justify this assumption. Inserting the approximation

$$\left(1 + \frac{\dot{\gamma}^*}{A}\right)^n \cong 1 + n\frac{\dot{\gamma}^*}{A} \tag{5}$$

into (2) yields

$$\tau^* = B\left(\frac{n}{A}\right)^{1/n}(\dot{\gamma}^*)^{1/n}. \tag{6}$$

Comparing (6) and (4), one may conclude that

$$m = \frac{1}{n}, \quad k = B\left(\frac{n}{A}\right)^{1/n}. \tag{7}$$

Hence, parameter n in the generalized model is somewhat equivalent to the reciprocal of power-law index and k is a combination of all parameters A, B, and n.

For Hershel-Buckley fluids, the constitutive relation is

$$\tau^* = \tau_0^* + k\dot{\gamma}^{*m}, \tag{8}$$

where τ_0^* is the initial yield stress for zero velocity gradient. For zero velocity gradient, there is no initial yield stress in (2) and the model does not cover Hershel-Buckley fluids for vanishing velocity gradients. For those fluids the more general form, i. e. (1), should be employed. Comparing (1) and (8), the initial yield stress can be defined as

$$\tau_0^* = \frac{B}{\delta^{1/n}}(\delta^n - 1)^{1/n}. \tag{9}$$

Parameter n in model (2) is dimensionless. In SI units, A should be the same unit as the velocity gradient, i. e. 1/s, and B should have the units of stress, i. e. Pa. In [1] nonstandard units are employed in presenting data of different gel water drilling fluids and gelex polymer mud. A has the units rpm and B has the units Ib/100ft^2. A is of magnitude 10^2 to 10^5 rpm while B is 10 to 10^3 Ib/100ft^2. n is in the range of 1.96 – 4.33. For details of the parameter values, the reader is referred to [1] not to reproduce his data.

Finally, (2) can be generalized to three dimensional flows in Cartesian coordinates

$$\tau_{xy}{}^* = B\left[\left(\frac{\left(\frac{\partial u^*}{\partial y^*} + \frac{\partial v^*}{\partial x^*}\right) + A}{A}\right)^n - 1\right]^{1/n},$$

$$\tau_{xz}{}^* = B\left[\left(\frac{\left(\frac{\partial u^*}{\partial z^*} + \frac{\partial w^*}{\partial x^*}\right) + A}{A}\right)^n - 1\right]^{1/n}, \tag{10}$$

$$\tau_{yz}{}^* = B\left[\left(\frac{\left(\frac{\partial v^*}{\partial z^*} + \frac{\partial w^*}{\partial y^*}\right) + A}{A}\right)^n - 1\right]^{1/n},$$

where u^*, v^*, and w^* are the velocity components in the x^*-, y^*-, and z^*-directions.

3. Pipe Flow

For pipe flow, the dimensional equation of motion can be written as follows:

$$\frac{\mathrm{d}p^*}{\mathrm{d}x^*} + \frac{1}{r^*}\frac{\mathrm{d}}{\mathrm{d}r^*}(\tau^* r^*) = 0. \tag{11}$$

The equation can be cast into a non-dimensional form

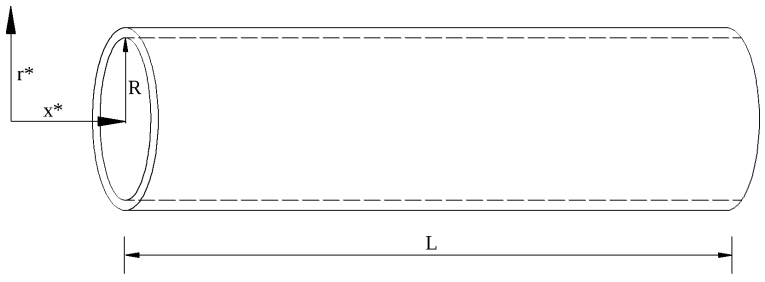

Fig. 1. Pipe flow geometry and coordinates.

through the relations

$$x=\frac{x^*}{L},\quad r=\frac{r^*}{R},\quad p=\frac{p^*}{(L/R)B},$$
$$u=\frac{u^*}{RA},\quad \tau=\frac{\tau^*}{B},\quad \dot\gamma=\frac{\dot\gamma^*}{A}, \tag{12}$$

where x is the axial coordinate, r is the radial coordinate, u is the axial velocity, R is the radius of the pipe, and L is the length of the pipe (see Fig. 1). The dimensionless equation of motion is

$$\frac{\mathrm{d}p}{\mathrm{d}x}+\frac{1}{r}\frac{\mathrm{d}}{\mathrm{d}r}(\tau r)=0. \tag{13}$$

In dimensionless quantities, model (2) can be expressed as

$$\tau=[(\dot\gamma+1)^n-1]^{1/n}, \tag{14}$$

where

$$\dot\gamma=-\frac{\mathrm{d}u}{\mathrm{d}r}. \tag{15}$$

The boundary conditions for the problem are

$$u(1)=0,\quad \frac{\mathrm{d}u}{\mathrm{d}r}(0)=0. \tag{16}$$

Substituting (15) into (14) and the result into (13), integrating the equation twice with the given boundary conditions, one finally obtains the velocity profile as follows:

$$u(r)=\int_1^r\left\{1-\left[1+\left(-\frac{r}{2}\frac{\mathrm{d}p}{\mathrm{d}x}\right)^n\right]^{1/n}\right\}\mathrm{d}r. \tag{17}$$

The discharge is $Q=\int_0^1 2\pi r u\,\mathrm{d}r$ or

$$Q=2\pi\int_0^1\left(r\int_1^r\left\{1-\left[1+\left(-\frac{\bar r}{2}\frac{\mathrm{d}p}{\mathrm{d}x}\right)^n\right]^{1/n}\right\}\mathrm{d}\bar r\right)\mathrm{d}r. \tag{18}$$

Equation (17) and (18) represent the velocity and discharge in an analytical integral form. For $n=1$, the velocity profile and discharge reduces to those of the Newtonian case in the dimensionless form [20]

$$u(r)=-\frac{1-r^2}{4}\frac{\mathrm{d}p}{\mathrm{d}x},\quad Q=-\frac{\pi}{8}\frac{\mathrm{d}p}{\mathrm{d}x}. \tag{19}$$

For some special n values, the integrals can be evaluated analytically. For $n=0.5$, the velocity profile is

$$u(r)=-\frac{1-r^2}{4}\frac{\mathrm{d}p}{\mathrm{d}x}+\frac{4}{3}\sqrt{-\frac{1}{2}\frac{\mathrm{d}p}{\mathrm{d}x}}(1-r^{3/2}). \tag{20}$$

For $n=0.5$, the discharge turns out to be

$$Q=2\pi\left\{-\frac{1}{16}\frac{\mathrm{d}p}{\mathrm{d}x}+\frac{2}{7}\sqrt{-\frac{1}{2}\frac{\mathrm{d}p}{\mathrm{d}x}}\right\}. \tag{21}$$

For $n=2$, the velocity profile is

$$u(r)=r-1-\frac{1}{2}\left\{r\sqrt{1+\left(-\frac{1}{2}\frac{\mathrm{d}p}{\mathrm{d}x}\right)^2r^2}-\sqrt{1+\left(-\frac{1}{2}\frac{\mathrm{d}p}{\mathrm{d}x}\right)^2}+\frac{\operatorname{Arc\,sinh}\left(-\frac{1}{2}\frac{\mathrm{d}p}{\mathrm{d}x}r\right)-\operatorname{Arc\,sinh}\left(-\frac{1}{2}\frac{\mathrm{d}p}{\mathrm{d}x}\right)}{-\frac{1}{2}\frac{\mathrm{d}p}{\mathrm{d}x}}\right\}. \tag{22}$$

For other n values, the integrals are numerically evaluated. In Figure 2, the velocity profiles are given for various pressure gradients for the $n=2$ case. In Figure 3, velocity profiles are contrasted with Newtonian and non-Newtonian cases with $n<1$. The non-Newtonian cases with $n>1$ are compared with Newtonian case in Figure 4. The velocities are higher for lower n values. Discharges are calculated in a similar way for a given pressure gradient and power index n. The results are summarized in Table 1. Discharges are obviously greater for higher pressure gradients. They are also higher for lower n values.

Table 1. Discharge values for pipe flow.

		n					
		0.25	0.5	1	2	3	4
dp/dx	-1	9.447	1.662	0.392	0.075	0.021	0.006
	-2	13.392	2.581	0.785	0.272	0.146	0.093
	-3	16.599	3.377	1.178	0.544	0.385	0.317

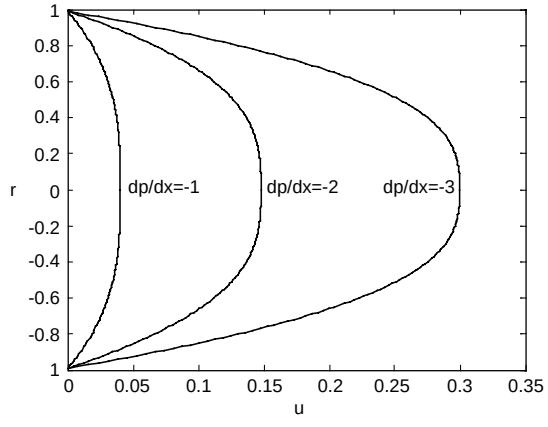

Fig. 2. Velocity profiles for pipe flow for various pressure gradients ($n = 2$).

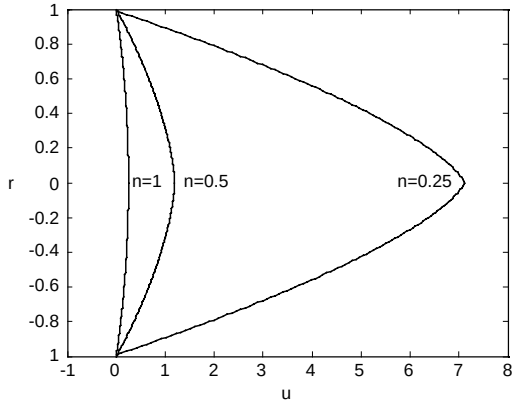

Fig. 3. Velocity profiles for pipe flow for $n < 1$ case ($dp/dx = -1$).

The results can be contrasted with the power-law approximation of the model. If the power-law approximation of shear stress given in (6) is rewritten in the dimensionless form

$$\tau = (n)^{1/n}(\dot{\gamma})^{1/n} \tag{23}$$

and substituted into (13), after similar calculations, the following velocity profile and discharge is obtained:

$$u(r) = \frac{1}{n(n+1)}\left(-\frac{1}{2}\frac{dp}{dx}\right)^n (1-r^{n+1}), \tag{24}$$

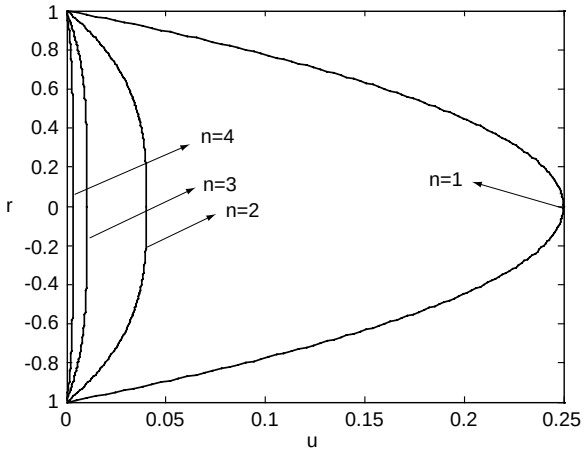

Fig. 4. Velocity profiles for pipe flow for $n > 1$ case ($dp/dx = -1$).

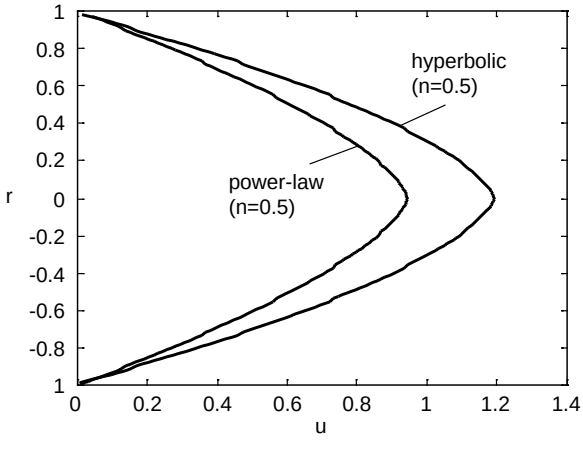

Fig. 5. Comparison of hyperbolic model with power-law approximation for pipe flow ($n = 0.5$).

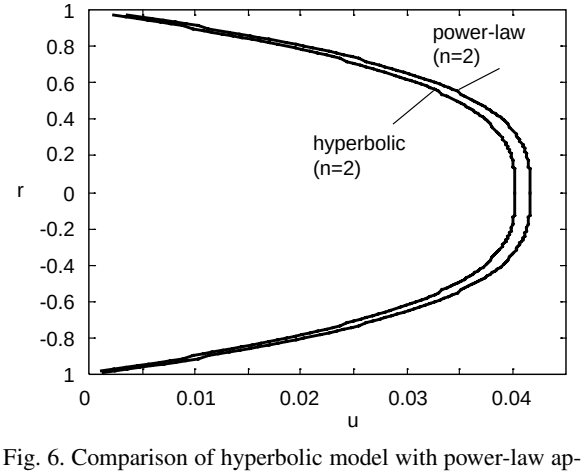

Fig. 6. Comparison of hyperbolic model with power-law approximation for pipe flow ($n = 2$).

$$Q = \frac{\pi}{n(n+3)} \left(-\frac{1}{2} \frac{\mathrm{d}p}{\mathrm{d}x} \right)^n. \tag{25}$$

The velocity profiles of the hyperbolic model are compared with their power-law approximations for $n = 0.5$ (Fig. 5) and $n = 2$ (Fig. 6). When $n < 1$, the power-law approximation underestimates the velocities and when $n > 1$, the power-law approximation overestimates the velocities.

4. Parallel Plate Flow

The geometry and coordinates selected are given in Figure 7. The dimensional equation of motion is

$$\frac{\mathrm{d}\tau^*}{\mathrm{d}y^*} = -\frac{\mathrm{d}p^*}{\mathrm{d}x^*}. \tag{26}$$

The non-dimensional terms are

$$\begin{aligned} &x = \frac{x^*}{L}, \quad y = \frac{y^*}{h}, \quad p = \frac{p^*}{(L/h)B}, \\ &u = \frac{u^*}{hA}, \quad \tau = \frac{\tau^*}{B}, \quad \dot{\gamma} = \frac{\dot{\gamma}^*}{A}, \end{aligned} \tag{27}$$

where x is the axial coordinate, y is the vertical coordinate, u is the axial velocity, $2h$ is the distance between the plates, and L is the length of the plates. The dimensionless equation of motion is

$$\frac{\mathrm{d}\tau}{\mathrm{d}y} = -\frac{\mathrm{d}p}{\mathrm{d}x}. \tag{28}$$

In dimensionless quantities, the shear stress and velocity gradients are

$$\tau = [(\dot{\gamma}+1)^n - 1]^{1/n}, \quad \dot{\gamma} = -\frac{\mathrm{d}u}{\mathrm{d}y}. \tag{29}$$

The boundary conditions for the problem are

$$u(1) = 0, \quad \frac{\mathrm{d}u}{\mathrm{d}y}(0) = 0. \tag{30}$$

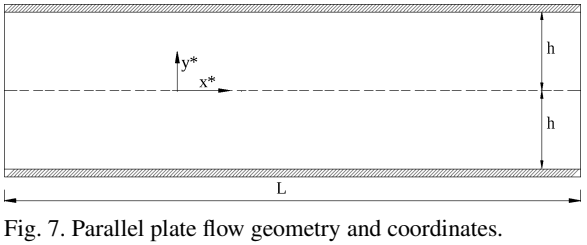

Fig. 7. Parallel plate flow geometry and coordinates.

Substituting (29) into (28), integrating twice with the given boundary conditions, one finally obtains the velocity profile as follows:

$$u(y) = \int_1^y \left\{ 1 - \left[1 + \left(-y \frac{\mathrm{d}p}{\mathrm{d}x} \right)^n \right]^{1/n} \right\} \mathrm{d}y. \tag{31}$$

For unit width, the discharge is $Q = 2\int_0^1 u \, \mathrm{d}y$ or

$$Q = 2 \int_0^1 \left(\int_1^y \left\{ 1 - \left[1 + \left(-\bar{y} \frac{\mathrm{d}p}{\mathrm{d}x} \right)^n \right]^{1/n} \right\} \mathrm{d}\bar{y} \right) \mathrm{d}y. \tag{32}$$

For $n = 1$, the velocity profiles and discharge reduces to those of Newtonian case in dimensionless form [20]

$$u(y) = -\frac{1-y^2}{2} \frac{\mathrm{d}p}{\mathrm{d}x}, \quad Q = -\frac{2}{3} \frac{\mathrm{d}p}{\mathrm{d}x}. \tag{33}$$

For some special n values, the integrals can still be evaluated analytically. For $n = 0.5$, the velocity profile is

$$u(y) = -\frac{1-y^2}{2} \frac{\mathrm{d}p}{\mathrm{d}x} + \frac{4}{3} \sqrt{-\frac{\mathrm{d}p}{\mathrm{d}x}} (1 - y^{3/2}). \tag{34}$$

For $n = 0.5$, the discharge turns out to be

$$Q = -\frac{2}{3} \frac{\mathrm{d}p}{\mathrm{d}x} + \frac{8}{5} \sqrt{-\frac{\mathrm{d}p}{\mathrm{d}x}}. \tag{35}$$

For $n = 2$, the velocity profile is

$$\begin{aligned} u(y) = y - 1 + \frac{1}{2\mathrm{d}p/\mathrm{d}x} &\left[\mathrm{Arc\,sinh} \left(-y \frac{\mathrm{d}p}{\mathrm{d}x} \right) \right. \\ &\left. - \mathrm{Arc\,sinh} \left(-\frac{\mathrm{d}p}{\mathrm{d}x} \right) \right] \\ - \frac{1}{2} &\left[y \sqrt{1 + \left(-y \frac{\mathrm{d}p}{\mathrm{d}x} \right)^2} - \sqrt{1 + \left(-\frac{\mathrm{d}p}{\mathrm{d}x} \right)^2} \right]. \end{aligned} \tag{36}$$

For other n values, integrals are numerically evaluated. In Figure 8, the velocity profiles are given for various pressure gradients for the $n = 2$ case. In Figure 9, velocity profiles are contrasted among Newtonian and non-Newtonian cases with $n < 1$. The non-Newtonian cases with $n > 1$ are compared with Newtonian cases

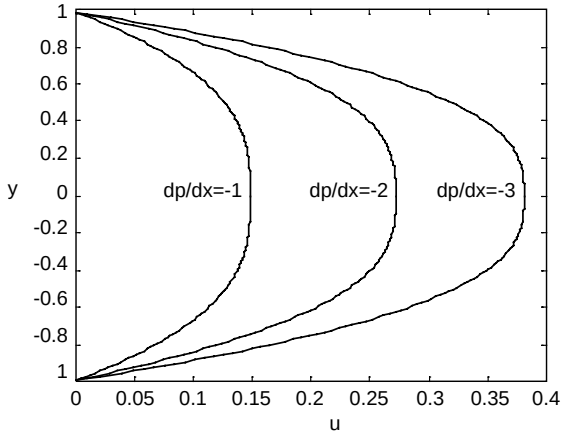

Fig. 8. Velocity profiles for parallel plate flow for various pressure gradients ($n = 2$).

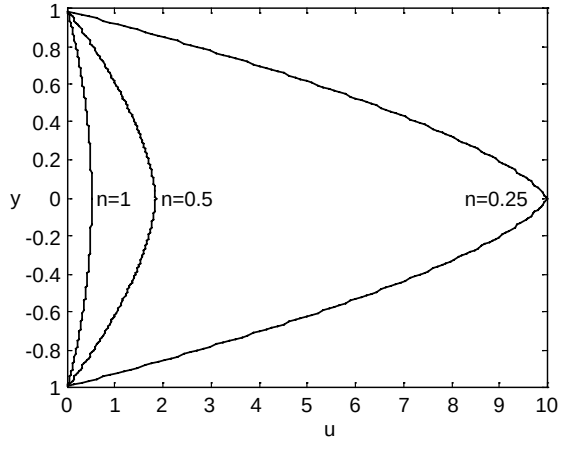

Fig. 9. Velocity profiles for parallel plate flow for $n < 1$ case ($\mathrm{d}p/\mathrm{d}x = -1$).

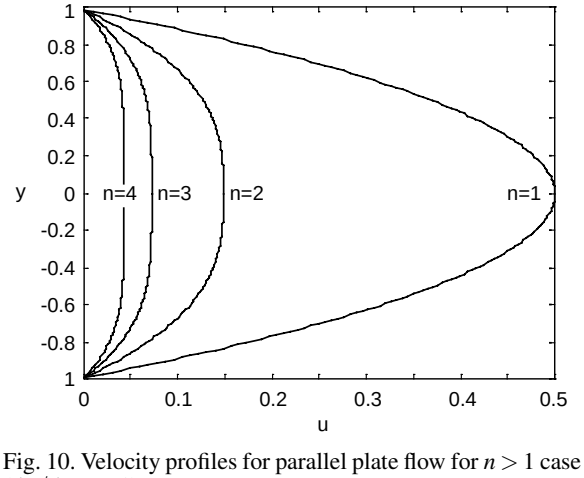

Fig. 10. Velocity profiles for parallel plate flow for $n > 1$ case ($\mathrm{d}p/\mathrm{d}x = -1$).

Table 2. Discharge values for parallel plate flow.

		n					
		0.25	0.5	1	2	3	4
$\mathrm{d}p/\mathrm{d}x$	-1	11.930	2.267	0.667	0.219	0.113	0.069
	-2	17.241	3.596	1.333	0.697	0.548	0.490
	-3	21.623	4.771	2.000	1.268	1.125	1.079

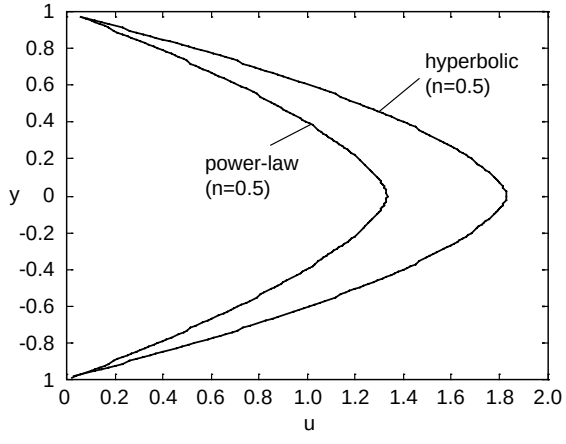

Fig. 11. Comparison of hyperbolic model with power-law approximation for parallel plate flow ($n = 0.5$).

in Figure 10. As can be seen from the figures, as n increases, the velocities drastically drop. The discharge is calculated in a similar way for a given pressure gradient and power index n. Results are summarized in Table 2. Discharges are higher for lower n values.

Similar to the analysis given in the previous section, results can be contrasted with the power-law approximation of the model. Power-law approximation of dimensionless shear stress is

$$\tau = (n)^{1/n}(\dot{\gamma})^{1/n}. \tag{37}$$

Inserting this shear stress into (28), after similar calculations, the following velocity profile and discharge is obtained:

$$u(y) = \frac{1}{n(n+1)}\left(-\frac{\mathrm{d}p}{\mathrm{d}x}\right)^n (1-y^{n+1}), \tag{38}$$

$$Q = \frac{2}{n(n+2)}\left(-\frac{\mathrm{d}p}{\mathrm{d}x}\right)^n. \tag{39}$$

The velocity profiles of the hyperbolic model are compared with their power-law approximations for $n = 0.5$ (Fig. 11) and $n = 2$ (Fig. 12). When $n < 1$, the power-law approximation underestimates the velocities and when $n > 1$, the power law approximation overestimates the velocities.

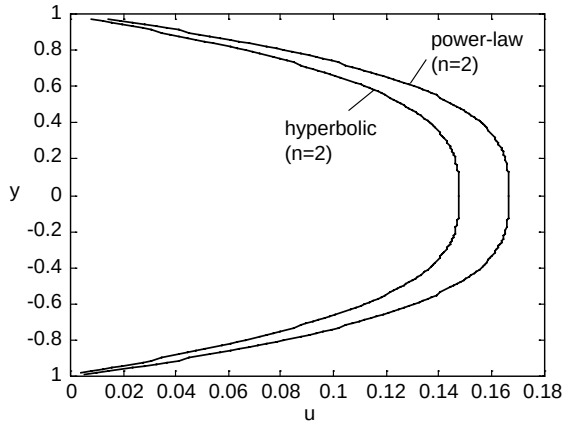

Fig. 12. Comparison of hyperbolic model with power-law approximation for parallel plate flow ($n = 2$).

5. Flow Between Rotating Concentric Cylinders

The geometry and coordinates selected are given in Figure 13. The inner cylinder is rotating with an angular velocity of Ω_1 and the outer cylinder is rotating with Ω_2 with the hyperbolic fluid placed between the cylinders. The dimensional equation of motion is

$$r^* \frac{\mathrm{d}\tau^*}{\mathrm{d}r^*} + 2\tau^* = 0. \tag{40}$$

The non-dimensional terms are defined as follows:

$$\begin{aligned} &r = \frac{r^*}{a}, \quad v = \frac{v^*}{\Omega_1 a}, \quad \tau = \frac{\tau^*}{B}, \\ &\dot{\gamma} = \frac{\dot{\gamma}^*}{\Omega_1}, \quad k_1 = \frac{b}{a}, \quad k_2 = \frac{\Omega_2}{\Omega_1}, \end{aligned} \tag{41}$$

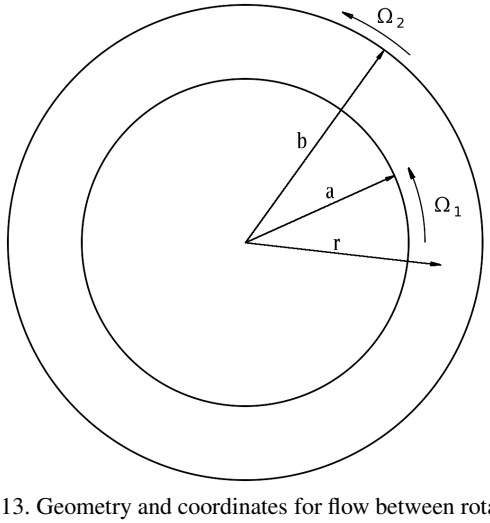

Fig. 13. Geometry and coordinates for flow between rotating concentric cylinders.

where r is the radial coordinate, θ is the angular coordinate, and $v_\theta(r) = v(r)$ is the velocity in the angular direction with variation only in the radial direction (no velocity components are assumed in the radial and vertical directions). The dimensionless equation of motion is

$$r\frac{\mathrm{d}\tau}{\mathrm{d}r} + 2\tau = 0. \tag{42}$$

In dimensionless quantities, the velocity gradient and shear stress are

$$\begin{aligned} &\dot{\gamma} = -\frac{v}{r} + \frac{\mathrm{d}v}{\mathrm{d}r}, \\ &\tau = \left\{ \left(\frac{\mathrm{d}v}{\mathrm{d}r} - \frac{v}{r} + 1 \right)^n - 1 \right\}^{1/n}. \end{aligned} \tag{43}$$

The dimensionless boundary conditions for the problem are

$$v(1) = 1, \quad v(k_1) = k_1 k_2. \tag{44}$$

Substituting (43) into (42) and rearranging, one finally obtains the equation of motion as follows:

$$r\frac{\mathrm{d}^2 v}{\mathrm{d}r^2} + \frac{\mathrm{d}v}{\mathrm{d}r} - \frac{v}{r} + 2 - 2\left(\frac{\mathrm{d}v}{\mathrm{d}r} - \frac{v}{r} + 1 \right)^{1-n} = 0. \tag{45}$$

For $n = 1$, this equation reduces to that of the Newtonian case [20]

$$r\frac{\mathrm{d}^2 v}{\mathrm{d}r^2} + \frac{\mathrm{d}v}{\mathrm{d}r} - \frac{v}{r} = 0. \tag{46}$$

For the general boundary conditions given in (44), the dimensionless analytical solution for the Newtonian case is

$$v(r) = \frac{k_1^2 k_2 - 1}{k_1^2 - 1} r + \frac{k_1^2 (1 - k_2)}{k_1^2 - 1} \frac{1}{r}. \tag{47}$$

For the original non-Newtonian problem, the solution is not simple. A linear solution $v(r) = cr$ satisfies the nonlinear problem for a restricted boundary condition, that is

$$v(r) = r \tag{48}$$

after applying (44). The solution is valid for the very restricted case of $k_2 = 1$ or $\Omega_2 = \Omega_1$. The linear solution, as expected, arises when both cylinders have the same angular velocities. This solution is numerically verified and irrespective of the n values, the linear solution is retrieved for $k_2 = 1$.

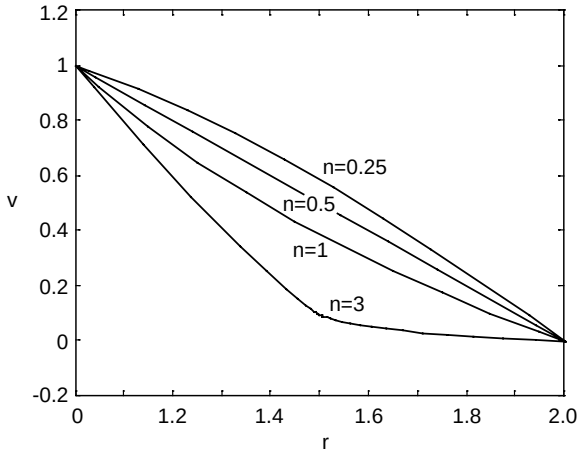

Fig. 14. Velocity profiles for flow between rotating cylinders for various power indexes with outer cylinder fixed ($k_1 = 2$, $k_2 = 0$).

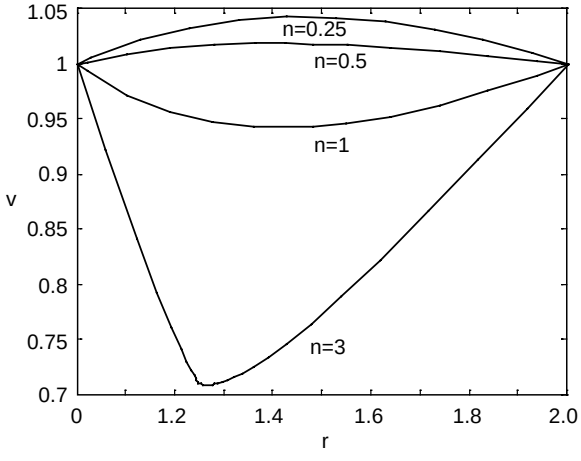

Fig. 15. Velocity profiles for flow between rotating cylinders for various power indexes with outer cylinder rotating slower ($k_1 = 2$, $k_2 = 0.5$).

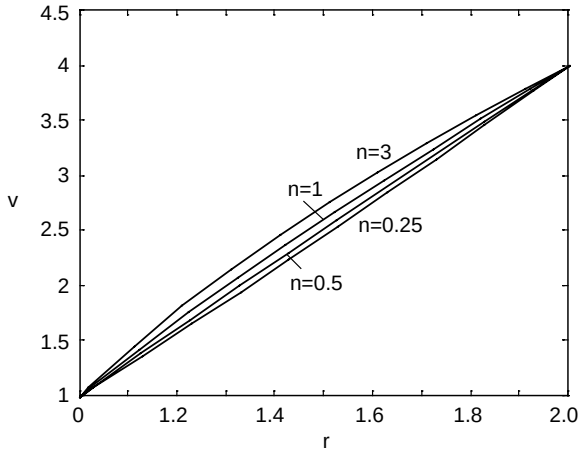

Fig. 16. Velocity profiles for flow between rotating cylinders for various power indexes with outer cylinder rotating faster ($k_1 = 2$, $k_2 = 2$).

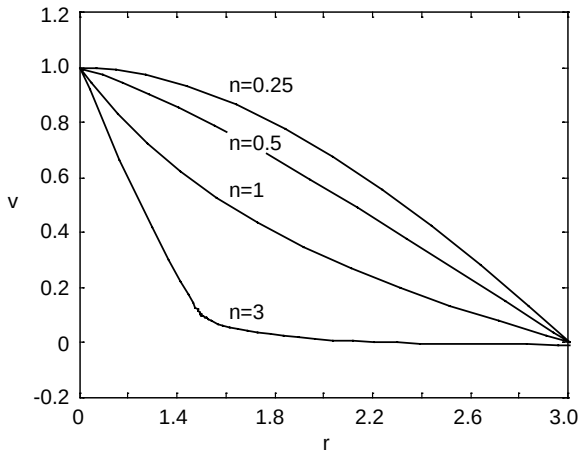

Fig. 17. Velocity profiles for flow between rotating cylinders for various power indexes with outer cylinder fixed ($k_1 = 3$, $k_2 = 0$).

Equation (45) is numerically integrated using a Runge-Kutta algorithm combined with shooting technique. Various n parameters are selected and the boundary conditions are varied by selecting different radius ratios k_1 and different angular velocity ratios k_2. Velocity profiles are given in Figures 14 – 19. In Figures 14 – 16, the radius ratio is selected as 2 (i. e. $k_1 = 2$). In Figure 14, the outer cylinder is fixed ($k_2 = 0$). Velocity profiles are plotted for four different power index values. A decrease in velocity is observed for increasing n. The $n < 1$ and $n > 1$ profiles are qualitatively different. In Figure 15, the outer cylinder is rotating slower ($k_2 = 0.5$), whereas in Figure 16, the outer cylinder is rotating faster ($k_2 = 2$) than the inner cylinder. Figure 16 is different from Figures 14 and 15. In Figures 14 and 15, as power index increases, the velocity drops, whereas in Figure 16 an increase in velocity is observed for an increase in power index n. With similar boundary conditions, for a radius ratio of 3 (i. e. $k_1 = 3$), Figures 17 – 19 are presented with similar trends.

For the power-law approximation of the model, the dimensionless shear stress is

$$\tau = n^{1/n}\left(-\frac{v}{r}+\frac{\mathrm{d}v}{\mathrm{d}r}\right)^{1/n}. \tag{49}$$

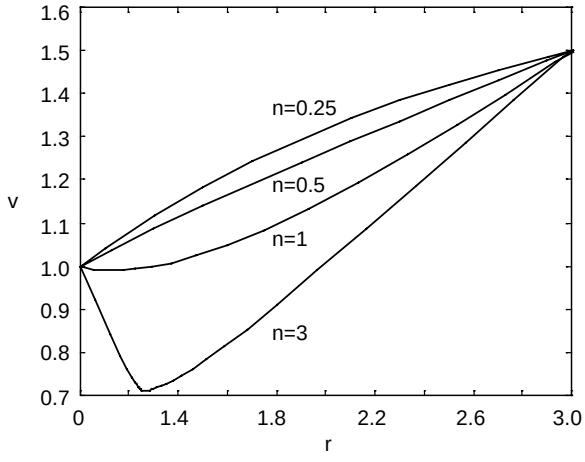

Fig. 18. Velocity profiles for flow between rotating cylinders for various power indexes with outer cylinder rotating slower ($k_1 = 3$, $k_2 = 0.5$).

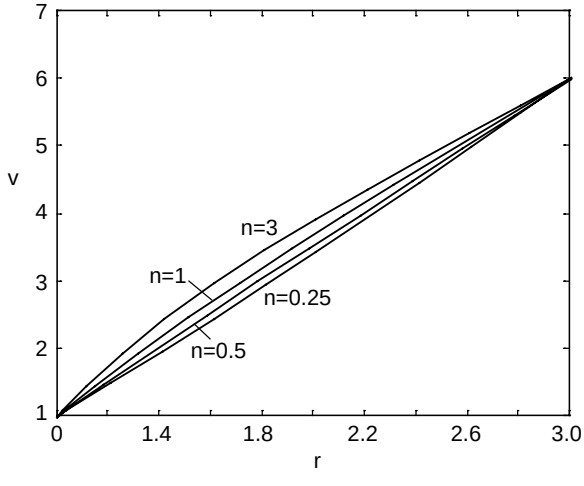

Fig. 19. Velocity profiles for flow between rotating cylinders for various power indexes with outer cylinder rotating faster ($k_1 = 3$, $k_2 = 2$).

Substitution into (42) yields

$$r\frac{\mathrm{d}^2 v}{\mathrm{d}r^2} + (1-2n)\left(\frac{v}{r} - \frac{\mathrm{d}v}{\mathrm{d}r}\right) = 0. \tag{50}$$

The solution of (50) for the boundary conditions (44) is

$$v = \frac{k_2 - k_1^{-2n}}{1 - k_1^{-2n}} r + \frac{1-k_2}{1-k_1^{-2n}} r^{1-2n}. \tag{51}$$

This velocity profile is contrasted with the numerical solutions of (45) for the generalized hyperbolic model in Figure 20 for $n = 3$, $k_1 = 4$, $k_2 = 0$. There is a qualitative difference between the decay of solutions, power-law approximation solution converges to zero more smoothly than the other solution.

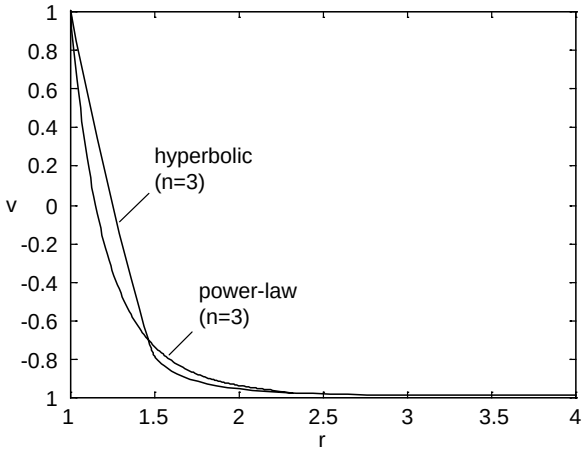

Fig. 20. Comparison of hyperbolic model with power-law approximation for flow between rotating cylinders ($k_1 = 4$, $k_2 = 0$, $n = 3$).

6. Concluding Remarks

A new hyperbolic non-Newtonian model with promising applications in Petroleum industry is considered. For this new model, three basic geometries are considered, namely, pipe flow, parallel plate flow, and flow between rotating cylinders. Analytical solutions in the form of integrals are presented for the first two cases and integrals are numerically evaluated to determine velocities and discharges. As the power index n in the model decreases, velocities and discharges increase. Direct numerical solutions of the resulting ordinary differential equation are presented for the last case. When the inner cylinder rotates faster, velocities increase for a decrease in power index n. On the contrary, when the outer cylinder rotates faster, velocities decrease for a decrease in power index n. For all three problems, the general hyperbolic model is also contrasted with its power-law approximation.

Acknowledgement

This work is supported by State Planning Agency of Turkey (DPT).

[1] S. M. Al-Zahrani, J. Petroleum Sci. Eng. **17**, 211 (1997).
[2] M. G. Timol and N. L. Kalthia, Int. J. Nonlinear Mech. **21**, 475 (1986).
[3] A. G. Hansen and T. Y. Na, ASME J. Basic Eng. **90**, 71 (1968).
[4] M. Pakdemirli, IMA J. Appl. Math. **50**, 133 (1993).
[5] J. E. Dunn and R. L. Fosdick, Arch. Rational Mech. Anal. **56**, 191 (1974).
[6] K. R. Rajagopal and R. L. Fosdick, Proc. Roy. Soc., London, Series A **369**, 351 (1980).
[7] M. Pakdemirli and E. S. Şuhubi, Int. J. Eng. Sci. **30**, 523 (1992).
[8] M. Pakdemirli, Int. J. Nonlinear Mech. **27**, 785 (1992).
[9] M. Pakdemirli, Int. J. Eng. Sci. **32**, 141 (1994).
[10] K. R. Rajagopal, A. Z. Szeri, and W. Troy, Int. J. Nonlinear Mech. **21**, 279 (1986).
[11] M. Massoudi and T. X. Phuoc, Acta Mech. **150**, 23 (2001).
[12] M. Ayub, T. Rasheed, and T. Hayat, Int. J. Eng. Sci. **41**, 2091 (2003).
[13] N. Ali, Y. Wang, and T. Hayat, Biorheology **45**, 611 (2008).
[14] T. Hayat, M. Sajid, and I. Pop, Nonl. Anal.: Real World Appl. **9**, 1811 (2008).
[15] T. Hayat, T. Javed, and M. Sajid, Phys. Lett. A **372**, 3264 (2008).
[16] T. Hayat, Z. Abbas, and M. Sajid, Phys. Lett. A **372**, 2400 (2008).
[17] T. Hayat, Z. Abbas, and N. Ali, Phys. Lett. A **372**, 4698 (2008).
[18] T. Hayat and Z. Abbas, ZAMP **59**, 124 (2008).
[19] S. M. Al-Zahrani and T. F. Al-Fariss, Chem. Eng. Processing **37**, 433 (1998).
[20] F. M. White, Fluid Mechanics, Mc Graw Hill, New York 1999.